Enhanced thermoelectric properties of p-type α-SrSi2 nanostructured by melt spinning

Rana Ghannam, Loic Coulomb, Adrien Moll, David Bérardan, Antonio Vieira E Silva, Benjamin Villeroy, Romain Viennois, Mickaël Beaudhuin

Enhanced thermoelectric properties of p-type α-$SrSi_2$ nanostructured by Melt Spinning

Rana Ghannam,[1] Loic Coulomb[1], Adrien Moll[2], David Bérardan[2], Antonio Vieira E Silva[1], Benjamin Villeroy[3], Romain Viennois[1], Mickaël Beaudhuin[1*]

[1] Institut Charles Gerhardt, Univ Montpellier, CNRS, ENSCM, 34095, Montpellier, France,

[2] ICMMO, Univ Paris Saclay, CNRS, UMR 8182, 914015, Orsay, France

[3]ICMPE, Univ Paris Est, CNRS, UMR 7182, 9432, Thiais, France

* Corresponding authors*: mickael.beaudhuin@umontpellier.fr*

Abstract

A melt spinning technique followed by spark plasma sintering technique was used to synthesize nanostructured $SrSi_2$ alloys with high homogeneity and density (>99%). The impact of the wheel speed on the microstructure of the ribbons was investigated and shows the presence of nanostructures. After sintering, typical grain size between ~140 and ~400 nm was obtained. We show that they permit to decrease strongly the lattice thermal conductivity. The ZT values of these melt-spun alloys are about two times higher than in our bulk material. We finally show that this short step process could be of strong interest for further development.

Keywords: Alkaline earth silicides, multi-scale approach, phonon scattering, melt spinning, rapid solidification

Introduction

We are facing growing urgency to transition towards cleaner and renewable energy alternatives. In this evolving landscape, technological innovations play a pivotal role. Breakthroughs in

energy storage, energy conversion, grid management, and efficiency improvements promise to reshape the energy sector. Among them thermoelectric devices can participate to this effort by converting waste heat into electrical energy and vice-versa [1]. Their performances are characterised by the dimensionless figure of merit $ZT= S^2\sigma T/(\lambda_l+\lambda_e)$ with S the Seebeck coefficient, σ the electrical conductivity, λ_L the lattice thermal conductivity and λ_e the electron thermal conductivity [1]. During the last years, the figure of merit of many materials have been improved between 1 and 2 [1]. However, most of them contain toxic and rare chemical elements such as Te, Se, Sb or Pb. Thus, many scientists have focused their work on thermoelectric materials such as oxides, sulphides or silicides to overwhelm this concern.

Indeed, silicides with semi-metallic or semiconducting behaviours have attracted much attention as they can be made of non-toxic, abundant and low-cost precursors [2]. Among them, the cubic α-$SrSi_2$ has been reported as either a Weyl semimetal with a pseudogap in the vicinity of the Fermi level E_F from some DFT calculations [3] or a narrow gap semiconductor (35 meV) referring to its negative temperature coefficient of resistivity [4]. Recent work reporting calculations with hybrid HSE06 exchange-correlation functionals as well as ARPES experiments have confirmed that cubic α-$SrSi_2$ is semiconducting [5]. Cubic α-$SrSi_2$ is one of the most promising thermoelectric silicide materials around room temperature [6]. Several approaches have been performed to optimize its performances, such as doping to improve both its power factor and the phonon scattering by mass defects [7]. This leads to a ZT up to 0.4 in α-$Sr_{0.92}Y_{0.08}Si_2$ at room temperature [8]. Despite these interesting results, the thermal conductivity is still rather large (3.8-5 W/m.K) excepted in defected Ca-alloyed α-$SrSi_2$ [9]. We have recently reduce the thermal conductivity of α-$SrSi_2$ down to 2.3 W/m.K at room temperature by nanostructuring through ball milling [10]. This permits to increase the ZT of pure α-$SrSi_2$ up to 0.2 at room temperature, the largest value so far for pure α-$SrSi_2$ [10]. Another way to reduce the lattice component of the thermal conductivity by nanostructuring is

the use of the melt spinning. This technique has been widely used for nanostructuring Skutterudites [11], $AgSbTe_2$ based-alloys [12] and others [13] with much success.

In the present study, nanostructuring by melt spinning followed by spark plasma sintering was used to study its impact on the thermoelectric properties of α-$SrSi_2$.

Materials and methods

Polycrystalline $SrSi_2$ samples were first synthesized using conventional arc-melting technique using Sr pieces (99.9%, Neyco) and Si lumps (99.9999%, Alfa Aesar) in stoichiometric amounts. The polycrystalline $SrSi_2$ alloys were nanostructured with melt spinning (MSP) experiment under Ar atmosphere in a MSP10 apparatus (Edmund Buhler GmbH, Germany) . The molten $SrSi_2$ is heated up to 1250 - 1330 °C in BN crucible and ejected onto a pure copper wheel (200 mm diameter) rotating from 30 to 60 rps leading to its rapid solidification. The cooling rates achievable by this equipment being in the order of 10^4-10^6 K/s. The ribbons obtain by MSP are grinded by hand with an agate molar pestle to keep the nanostructure.

After melt spinning, Spark Plasma Sintering (SPS) technique was used to prepare dense pellet using a DR Sinter Lab 515S (Fuji Electronics, Japan) at ICMPE (Paris, France). Tungsten carbide die is used to obtain pellets of 8 mm of diameter. Uniaxial pressure of 200 MPa and DC pulses were applied at both sides. A dwell time of 5 or 30 min was applied at 800°C. Each pellets have been characterized individually for structural, chemical and physical characterization.

The samples were analysed by using an X-Ray Diffraction apparatus Philips X′Pert, CuKα1 and CuKα2 ($\lambda_{K\alpha1}$= 0, 15406 nm et $\lambda_{K\alpha2}$= 0, 15444 nm). The XRD patterns were analysed by pattern matching and Rietveld refinement using Fullprof software [14]. The crystallite size and the microstrain are determined using the Williamson Hall formula implemented in Fullprof software.

The microstructure was analysed by scanning electron microscopy (SEM) with a Hitachi S4800 apparatus (Hitachi High-Tech Corporation, Tokyo, Japan). EDX analysis was done on melt spun ribbons and confirmed the 1:2 stoichiometry.

The total thermal conductivity (λ_{tot} = αdCp) was derived from the thermal diffusivity α measured cross plane by the laser flash method from Netzsch (LFA 467 Hyperflash, Netzsch, Selb, Germany), the density d determined with the Archimedes method and the heat capacity Cp measured with a DSC 404 C Pegasus de Netzch (Netzsch, Selb, Allemagne). The uncertainty is estimated to be ±2.5% [15].

Electrical resistivity and Seebeck coefficients were measured respectively on plane and cross plane with homemade apparatus, the uncertainty is estimated to be less than 10% [15].

Results and discussion

The XRD patterns and the images of the ribbons obtained by MSP before and after sintering are given in Fig. 1 and Fig. 2 respectively. The sample obtained after arc melting was mentioned as 'Bulk'. First, we observed that after melt spinning the samples are mainly composed of the α-$SrSi_2$ phase and no β-$SrSi_2$ is detected in the limit of detection of the equipment. From Rietveld refinement (Table 1) one observes that the unit cell of MSP samples increases slightly compared to the bulk a = 6.5340(3) Å [10] and that the crystallite size decreases with increasing the wheel speed from about 400 to 60 nm whereas the microstrain remains low (about 0.05%). After SPS, the pellets have a relative density above 99 % and a very weak amount of secondary phases as β-$SrSi_2$, SrSi and Si appeared (Fig. 2). One notice that the lattice parameter decreases for 30 rps and 45 rps samples whereas it increases slightly for 60 rps ones. In order to study the influence of the nanostructuring on the thermoelectric performances, the sample Bulk-SPS5 is considered as our reference, it was sintered directly after arc melting without being nanostructured by melt spinning. From Table 1 one observes that the crystallite size increase by a factor 2 or 3 whatever is the SPS dwell (5 or 30 minutes) reaching about 400 nm after 30

rps to about 150 nm after 45 and 60 rps. It is interesting to notice that the microstrain increase after SPS and could be explained by the stress induced by this sintering process as already observed in [16].

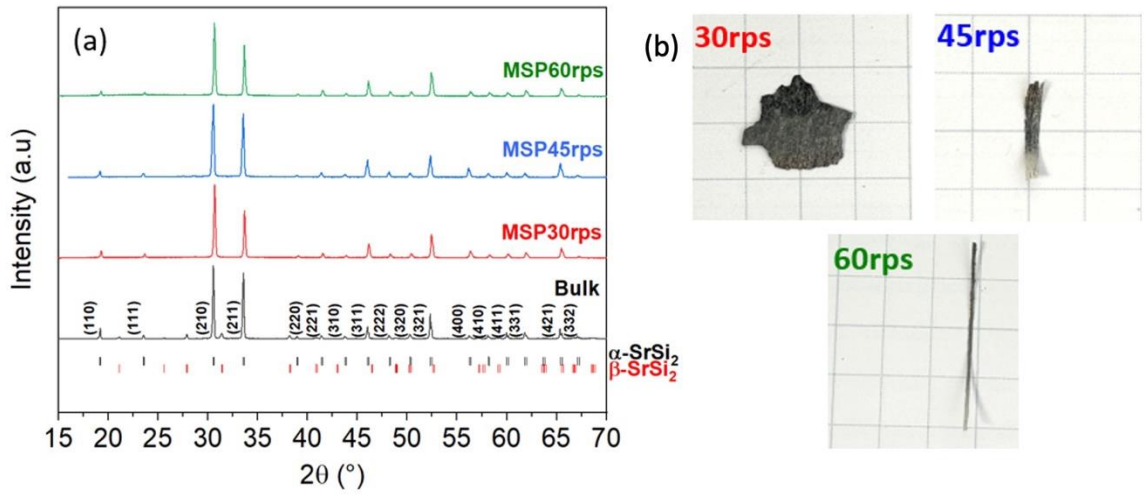

Figure 1: Diffraction pattern (a) and images (b) of α-$SrSi_2$ melt spinned at 30, 45 and 60 rps

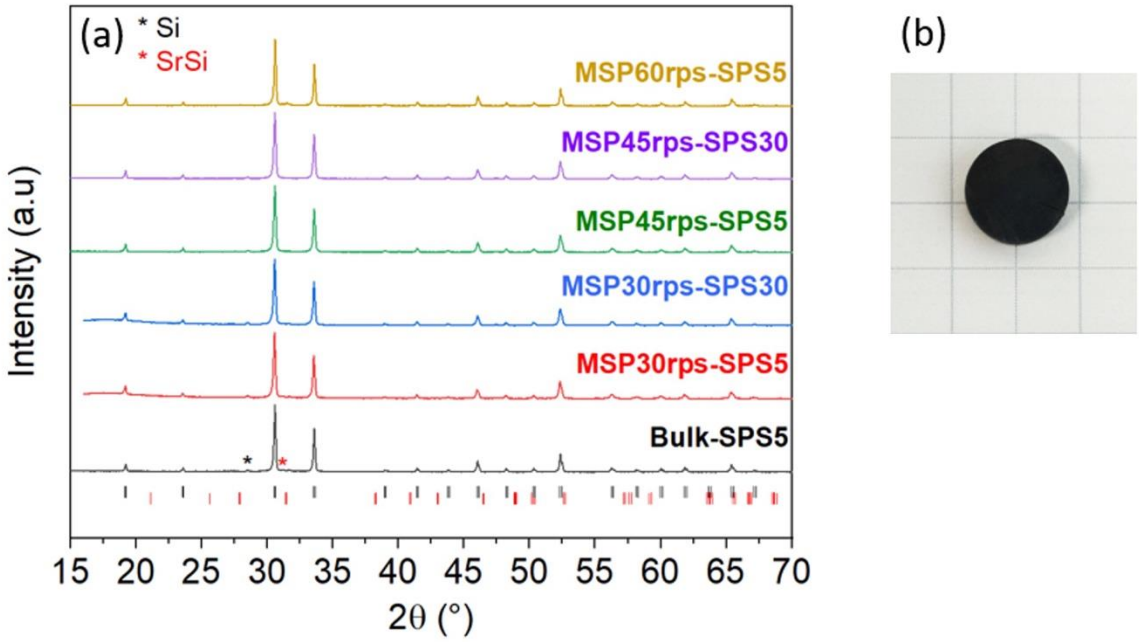

Figure 2: Diffraction pattern (a) of α-$SrSi_2$ melt spinned at 30, 45 and 60 rps and then sintered using SPS technique with dwell time of 5 and 30 min. In (b) an image to a pellet after SPS. Note that all the pellets are similar after SPS

The SEM images of the ribbons are given in Fig. 3. It is observed that the microstructure becomes more textured when increasing the wheel speed. We can also observe a higher density by going from 30 rps to 60 rps. Cross section measurement enables to determine the thickness of the ribbons (Fig. 3). It was ranging from 40 µm to 4 µm while increasing the wheel speed from 30 to 60 rps.

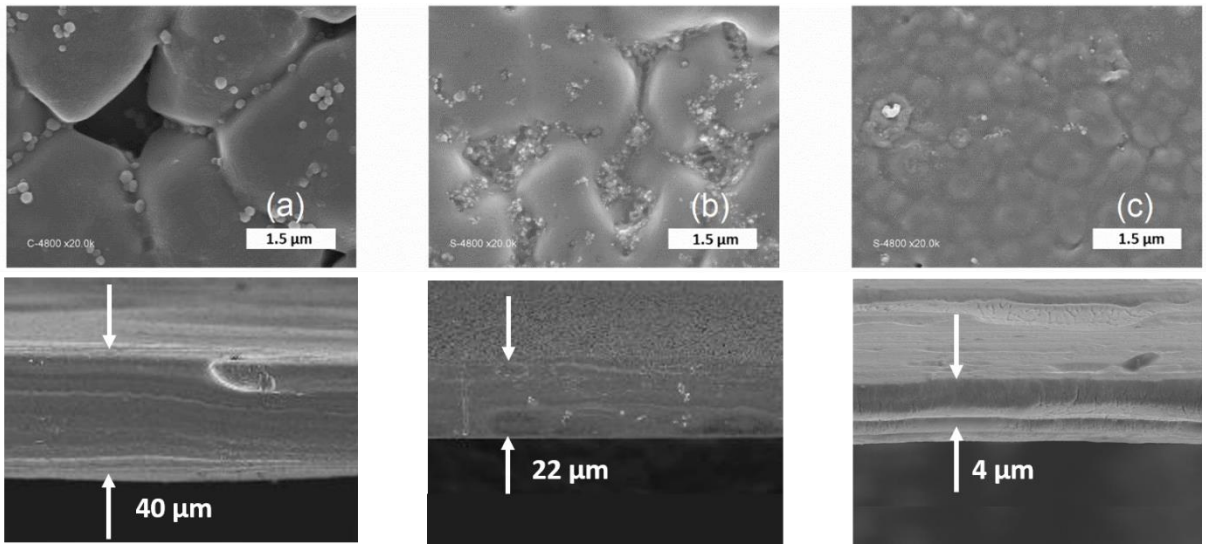

Figure 3: Secondary electron images of α-$SrSi_2$ melt spun ribbons at (a) 30 rps,(b) 45 rps and (c) 60 rps

Table 1: Melt spun sample at 30, 45 and 60 rps and their pellets sintered at 5 (SPS5) and 30 min (SPS30) and their lattice parameter, crystallite size, microstrain.

Sample	Lattice parameter (Å)	Crystallite size (nm)	Microstrain (%)
MSP30rps	6.5405 (1)	220(1)	0.05 (1)
MSP30rps-SPS5	6.5341(0)	400(2)	0.27(1)
MSP30rps-SPS30	6.5342(1)	395(4)	0.28(1)
MSP45rps	6.5437(0)	60(1)	0.04(1)
MSP45rps-SPS5	6.5352(1)	140(1)	0.23(1)
MSP45rps-SPS30	6.5356(1)	170(0)	0.23(1)
MSP60rps	6.5397(1)	60(1)	0.03(1)
MSP60rps-SPS5	6.5416(1)	150(1)	0.19(0)

Thermoelectric properties

The temperature-dependent Seebeck coefficient and electrical resistivity between 300 and 600 K are given in Fig. 4.

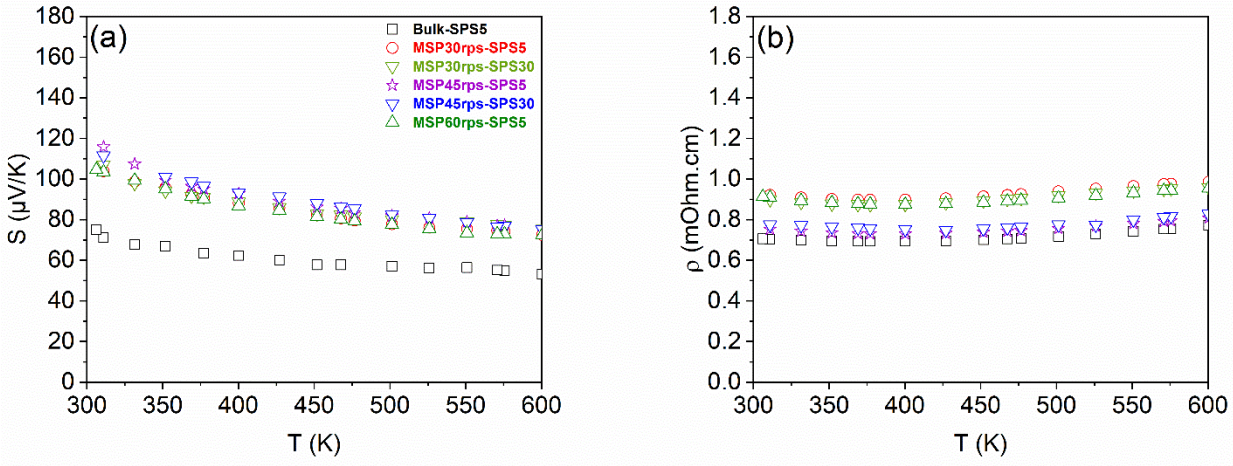

Figure 4: Seebeck coefficient (a) and electrical resistivity (b) of α-$SrSi_2$ poly and nanostructured by melt spinning 30, 45 and 60 rps between 300 K and 600 K

The electrical resistivity decreases with increasing temperature (up to about 400 K) and then increases which is related to the very narrow bandgap of α-$SrSi_2$. Imai et al. have highlighted that, at temperatures below 400 K, the decrease of the electrical resistivity with temperature owing to the thermal activation of charge carriers across the bandgap. This characterizes the intrinsic regime. Conversely, at temperatures exceeding 400 K, the thermal energy (34.4 meV) equals or surpasses the bandgap energy (35 meV). In this scenario, a majority of charge carriers are activated, leading to an almost constant intrinsic charge carrier density and a rise in electrical resistivity with increasing temperature [4].

We can notice, that after MSP, the Seebeck coefficient was increased from 75 to attend a maximum of 116 µV/K for the ribbons obtained at 45 rps. This increase could be assigned either to a modification of the electronic band feature of α-$SrSi_2$ due to the creation of defects during the MSP, akin to the influence of resonant levels [18] or to a change of the charge carrier concentration. As α-$SrSi_2$ is semiconducting with small energy bandgap, it is necessary to take

into account the contribution from minority charge carriers and to use a two bands model for understanding the variation of the Seebeck coefficient [17]. In this case a two bands model, the total Seebeck coefficient S_{tot} is:

$$S_{tot} = \frac{S_e\sigma_e + S_h\sigma_h}{\sigma_e + \sigma_h}$$

with S_h and σ_h being the Seebeck coefficient and the electrical conductivity of the holes, here the majority charge carriers, and S_e and σ_e being the Seebeck coefficient and the electrical conductivity of the electrons, here being the minority charge carriers. For determining the best scenario, it will be necessary to perform both Hall effect and magnetoresistance experiments at high magnetic field, as well as function of the temperature in order to obtain the majority and minority charge carriers concentrations and mobilities. This is however beyond the scope of the present work.

An optimum power factor at 300 K was obtained for ribbons spun at 45 rps (1.78 $mW.m^{-1}.K^{-2}$) as shown in Fig. 5. This is significantly larger than the PF obtained for the samples nanostructured by ball milling with Sr of 3N purity reported in our previous work [10] but smaller than the PF reported by Singh et al for pure $SrSi_2$ obtained with Sr of 3N purity [5].

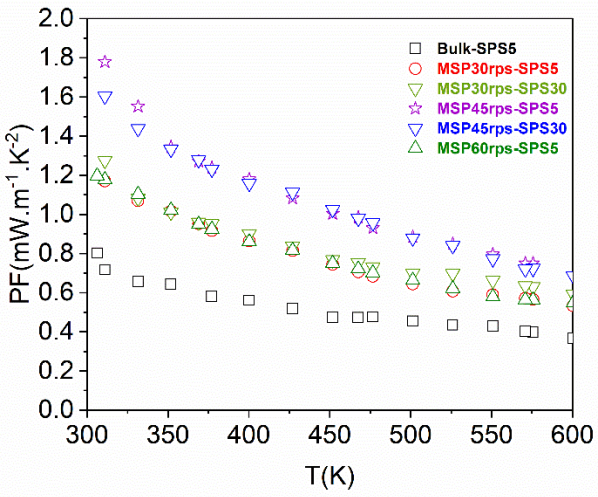

Figure 5: Power factor of α-$SrSi_2$ poly and nanostructured by melt spinning 30, 45 and 60 rps between 300 K and 600 K

The thermal conductivity data of these samples are given in Fig. 6. As crystallite sizes remain too large to have a significant effect on the thermal conductivity, we didn't notice strong modification with the reference sample except for the ribbons spun at 60 rps whose total thermal conductivity was decreased from 4.3 to 3.66 $W.m^{-1}.K^{-1}$ around 300K (Fig. 6). It is noteworthy that the effect of melt spinning on the thermal conductivity of α-$SrSi_2$ is significantly less pronounced compared to the impact of ball-milling for nanostructuring [10].

The electronic thermal conductivity (Fig. 6(a)) of α-$SrSi_2$ has been determined using the Wiedemann-Franz law [19] $\lambda_e = L_0 \sigma T$, with the Lorenz number L_0 of α-$SrSi_2$ equal to [20]:

$$L_0 = 1.49 - 0.49\, e^{-|S|/21} + 1.4\, e^{-|S|/85} \quad (1)$$

This equation is obtained using the single parabolic band approximation and acoustical phonon scattering. Previously, Imai et al [4] has shown that the mobility follows the temperature dependence expected for the acoustical phonon scattering above 200 K. After subtracting the electronic thermal conductivity to the total thermal conductivity, one obtains the lattice thermal conductivity (Fig. 6(b)). Note that its increases above 500 K due to the bipolar contribution as in the case of the samples obtained from ball-milling [10].

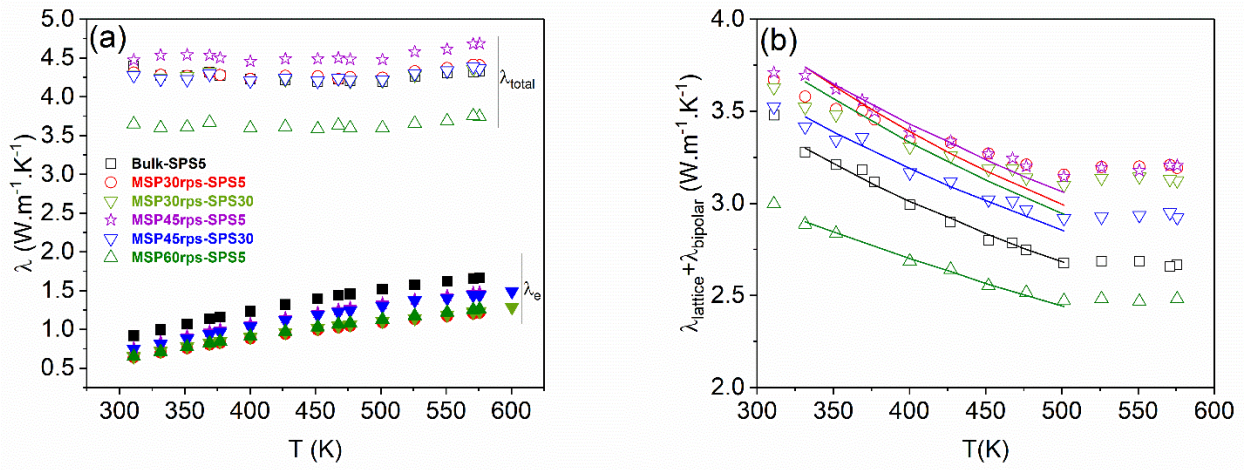

Figure 6: Thermal conductivity (a) and lattice and bipolar thermal conductivity (b) of α-$SrSi_2$ poly and nanostructured by melt spinning 30, 45 and 60 rps between 300 K and 600 K. In (b), symbols and lines refer to experimental and fitted data respectively

In order to understand the impact of the scattering parameters on the thermal conductivity of α-$SrSi_2$, we model the lattice thermal conductivity of α-$SrSi_2$ using the Klemens-Callaway's model with relaxation times from point defect scattering, umklapp scattering and boundary grain scattering [21–23] as discussed previously in [24].

In the Klemens-Callaway's model, the thermal conductivity can be expressed as [21–23]:

$$\kappa_l(T) = \frac{k_B}{2\pi^2 v}\left(\frac{k_B T}{\hbar}\right)^3 \int_0^{\theta_D/T} \frac{x^4 e^x}{\tau_C^{-1}(e^x-1)^2}\,dx \qquad (1)$$

with $x = \hbar\omega/k_B T$, ω the phonon frequency, k_B the Boltzmann constant, $\hbar$ the reduced Planck constant, θ_D the Debye temperature (380 K [25]), v the sound velocity (3620 m/s [25]) and τ_C the phonon scattering relaxation time. The phonon scattering relaxation time is obtained using the Matthiessen's rule and the relaxation time from the different phonon scattering mechanisms. The inverse of the phonon scattering relaxation time can expressed as:

$$\tau_C^{-1} = A\omega^4 + B\omega^2 T + \frac{v}{D} \qquad (2)$$

with $A = \frac{V_0 \Gamma}{4\pi v^3}$ (Γ is the impurity scattering parameter and V_0 is the volume per atom), $B = \frac{2\gamma^2 k_B}{\mu V_0 \omega_D}$ (γ is the Gruneisen anharmonicity parameter, μ is the shear modulus and ω_D is the Debye frequency) and D is the crystallite size.

In our modelling, we first fit the bulk α-$SrSi_2$ compound with A and B as variable and with D = 1 µm. To notice, higher grain size does not modify significantly the fitting parameters. For the samples obtained by melt spinning and SPS we fixed the prefactor B to 2.74 10^{-18} s/K for the phonon-phonon Umklapp scattering as it is an intrinsic parameter of α-$SrSi_2$. The value of D was set to the crystallite size obtained from the XRD refinement and finally only the A parameter is fitted. The results are the solid lines in Fig. 6 (b) and the fitting parameters are shown in the Table 3. From sample Bulk-SPS5 to 30 and 45 rps one notices a decrease of the point defect scattering related to a decrease of the crystallite size and an increase of the

microstrain as already shown in Table 1. These observations could explain the increase of the lattice thermal conductivity observed for these nanostructured samples. However, one notices that for 45 rps and 60 rps samples the point defect scattering increases whereas the crystallite size is similar. This behaviour could explain the strong decrease of the lattice thermal conductivity compared to bulk samples.

Table 3: Fitted parameters obtained from Callaway modelling for melt spun samples

	A (10^{-42} s^3)	**B (10^{-18} s/K)**	**D (µm)**
Bulk-SPS5	7.2	2.74	1
MSP30rps-SPS5	4.46	2.74	0.4
MSP30rps-SPS30	4.22	2.74	0.4
MSP45rps-SPS5	3.03	2.74	0.140
MSP45rps-SPS30	3.74	2.74	0.170
MSP60rps-SPS5	5.04	2.74	0.150

As discussed above 45 rps has the higher power factor and 60 rps has the lowest thermal conductivity which leads to a compensation between the power factor and the thermal conductivity giving quite similar figure of merit (See Fig. 7). However, one could notice that the figure of merit is strongly improved from 0.05 to 0.12 after 45 rps at 300K. This value is similar to the ZT obtained for ball-milled samples with Sr of 3N purity in our previous work. However, this process is much faster to get large amount of nanostructured samples. Further optimisation can be achieved with a multiscale approach by combining both doping and nano-structuring.

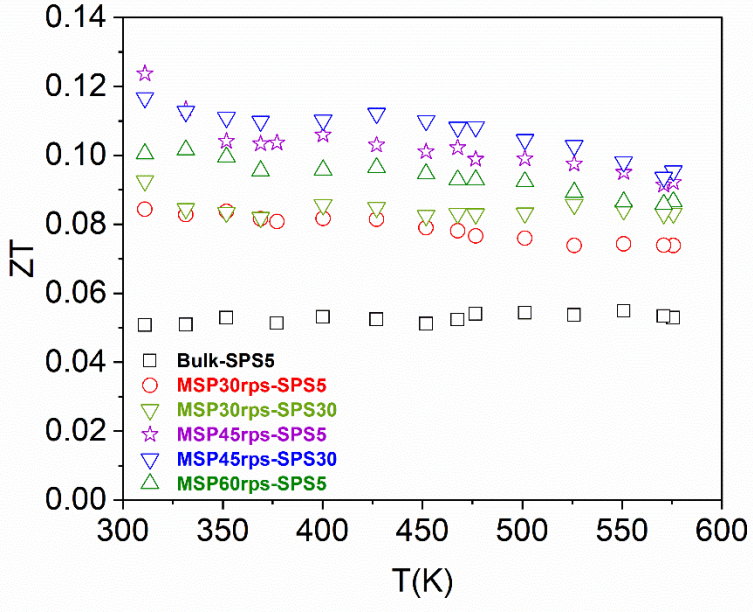

Figure 7: Figure of merit of α-$SrSi_2$ poly and nanostructured by melt spinning 30, 45 and 60 rps between 300 K and 600 K

Conclusion

We successfully produced nanostructured α-$SrSi_2$ ribbons using the high cooling rate of the melt-spinning process and the rapid densification of spark plasma sintering. The MSP-SPS samples demonstrated a higher Seebeck coefficient and increased electrical resistivity compared to the polycrystalline sample. Although the total thermal conductivity slightly decreased with 60 rps samples, the thermoelectric performance of the MSP-SPS sample significantly improved. At room temperature, a ZT value of 0.12 was achieved, approximately twice as high as that of our bulk sample. Our findings suggest that the nanostructures obtained through MSP introduce a new scattering mechanism, significantly influencing electron and phonon transport properties. Therefore, it is reasonable to consider this approach as a new paradigm for designing and optimizing thermoelectric materials.

Acknowledgment

We would like to thank the ANR-19-CE05-0001 for its financial support, Didier Cot and Bertrand Rebière for SEM images.

References

[1] T. Zhu, Y. Liu, C. Fu, J.P. Heremans, J.G. Snyder, X. Zhao, Compromise and Synergy in High-Efficiency Thermoelectric Materials, Advanced Materials. 29 (2017). https://doi.org/10.1002/adma.201605884.

[2] A. Nozariasbmarz, A. Agarwal, Z.A. Coutant, M.J. Hall, J. Liu, R. Liu, A. Malhotra, P. Norouzzadeh, M.C. Öztürk, V.P. Ramesh, Y. Sargolzaeiaval, F. Suarez, D. Vashaee, Thermoelectric silicides: A review, Jpn J Appl Phys. 56 (2017). https://doi.org/10.7567/JJAP.56.05DA04.

[3] B. Singh, G. Chang, T.-R. Chang, S.-M. Huang, C. Su, M.-C. Lin, H. Lin, A. Bansil, Tunable double-Weyl Fermion semimetal state in the SrSi$_2$ materials class, Sci Rep. (2018). https://doi.org/10.1038/s41598-018-28644-y.

[4] M. Imai, T. Naka, T. Furubayashi, H. Abe, T. Nakama, K. Yagasaki, Electrical properties of polycrystalline SrSi2, Appl Phys Lett. 86 (2005). https://doi.org/10.1063/1.1849423.

[5] K. Manna, N. Kumar, S. Chattopadhyay, J. Noky, M. Yao, J. Park, T. Förster, M. Uhlarz, T. Chakraborty, B. V. Schwarze, J. Hornung, V.N. Strocov, H. Borrmann, C. Shekhar, Y. Sun, J. Wosnitza, C. Felser, J. Gooth, Three-dimensional quasiquantized Hall insulator phase in SrSi2, Phys Rev B. 106 (2022) L041113. https://doi.org/10.1103/PhysRevB.106.L041113.

[6] S.K. Singh, M. Imai, Thermoelectric properties of cubic Ba-substituted strontium disilicide, Sr1-xBaxSi2, with Ba content above solid solubility limit, Intermetallics (Barking). 127 (2020) 106981. https://doi.org/10.1016/j.intermet.2020.106981.

[7] Y.K. Kuo, B. Ramachandran, C.S. Lue, Optimization of thermoelectric performance of SrSi2-based alloys via the modification in band structure and phonon-point-defect scattering, Front Chem. 2 (2014) 106. https://doi.org/10.3389/fchem.2014.00106.

[8] C.S. Lue, M.D. Chou, N. Kaurav, Y.T. Chung, Y.K. Kuo, Enhancement in the thermoelectric performance by Y substitution on SrSi2, Appl Phys Lett. 94 (2009). https://doi.org/10.1063/1.3136847.

[9] C.S. Lue, Y.S. Tseng, J.Y. Huang, H.L. Hsieh, H.Y. Liao, Y.K. Kuo, Low lattice thermal conductivity suppressed by Sr-deficiency in Sr0.9Ca0.1Si2, AIP Adv. 3 (2013) 072132. https://doi.org/10.1063/1.4817576.

[10] R. Ghannam, A. Moll, D. Bérardan, L. Coulomb, A. Vieira-E-Silva, B. Villeroy, R. Viennois, M. Beaudhuin, Impact of the nanostructuring on the thermal and thermoelectric properties of α-SrSi2, Journal of Alloys and Compounds. 968 (2023) 171876. https://doi.org/10.1016/j.jallcom.2023.171876.

[11] X.G. Li, W. Di Liu, S.M. Li, D. Li, H. Zhong, Z.G. Chen, Impurity Removal Leading to High-Performance CoSb3-Based Skutterudites with Synergistic Carrier Concentration Optimization and Thermal Conductivity Reduction, ACS Applied Materials and Interfaces. 13 (2021) 54185–54193. https://doi.org/10.1021/acsami.1c16622.

[12] B. Du, H. Li, J. Xu, X. Tang, C. Uher, Enhanced thermoelectric performance and novel nanopores in AgSbTe 2 prepared by melt spinning, Journal of Solid State Chemistry. 184 (2011) 109–114. https://doi.org/10.1016/j.jssc.2010.10.036.

[13] A. Melnikov, Powder metallurgy for thermoelectrics, Metal Powder Report. 71 (2016) 279–284. https://doi.org/10.1016/j.mprp.2016.05.008.

[14] L.W. Finger, D.E. Cox, A.P. Jephcoat, Correction for powder diffraction peak asymmetry due to axial divergence, J Appl Crystallogr. 27 (1994) 892–900. https://doi.org/10.1107/S0021889894004218.

[15] E. Alleno, D. Bérardan, C. Byl, C. Candolfi, R. Daou, R. Decourt, E. Guilmeau, S. Hébert, J. Hejtmánek, B. Lenoir, A round Robin test of the uncertainty on the measurements of the thermoelectric dimensionless figure of merit of Co0.97Ni0.03Sb3, (2015). https://doi.org/10.1063/1.4905250ï.

[16] W.R. Matizamhuka, Spark plasma sintering (SPS) - An advanced sintering technique for structural nanocomposite materials, Journal of the Southern African Institute of Mining and Metallurgy. 116 (2016) 1171–1180. https://doi.org/10.17159/2411-9717/2016/v116n12a12.

[17] H. Naithani, E. Müller, J. De Boor, Developing a two-parabolic band model for thermoelectric transport modelling using Mg2Sn as an example, JPhys Energy. 4 (2022) 0–13. https://doi.org/10.1088/2515-7655/ac7fb8.

[18] J.P. Heremans, B. Wiendlocha, A.M. Chamoire, Resonant levels in bulk thermoelectric semiconductors, Energy and Environmental Science. 5 (2012) 5510–5530. https://doi.org/10.1039/c1ee02612g.

[19] X.F. Zheng, C.X. Liu, Y.Y. Yan, Q. Wang, A review of thermoelectrics research - Recent developments and potentials for sustainable and renewable energy applications, Renewable and Sustainable Energy Reviews. 32 (2014) 486–503. https://doi.org/10.1016/j.rser.2013.12.053.

[20] H.S. Kim, Z.M. Gibbs, Y. Tang, H. Wang, G.J. Snyder, Characterization of Lorenz number with Seebeck coefficient measurement, APL Mater. 3 (2015) 1–6. https://doi.org/10.1063/1.4908244.

[21] J. Callaway, Model for lattice thermal conductivity at low temperatures, Physical Review. 113 (1959) 1046–1051. https://doi.org/10.1103/PhysRev.113.1046.

[22] Measurements 1433, 7 (1962).

[23] P.G. Klemens, The scattering of low-frequency lattice waves by static imperfections, Proceedings of the Physical Society. Section A. 68 (1955) 1113–1128. https://doi.org/10.1088/0370-1298/68/12/303.

[24] M. Khalil, A. Moll, M. Godfroy, A. Letrouit-Lebranchu, B. Villeroy, E. Alleno, R. Viennois, M. Beaudhuin, Thermoelectric properties and stability of nanostructured chromium disilicide CrSi2, J Appl Phys. 126 (2019). https://doi.org/10.1063/1.5117152.

[25] K. Hashimoto, K. Kurosaki, Y. Imamura, H. Muta, S. Yamanaka, Thermoelectric properties of BaSi2, SrSi2, and LaSi, J Appl Phys. 102 (2007) 063703. https://doi.org/10.1063/1.2778747.